J. Fluid Mech. (1973), *vol.* 57, *part* 4, *pp.* 739–752
Printed in Great Britain

Surface relief accompanying natural convection in liquid pools heated from below

By WILLIAM V. KAYSER† AND JOHN C. BERG
Department of Chemical Engineering, University of Washington, Seattle

(Received 31 May 1972)

Free-surface deformations accompanying natural convection in shallow liquid pools heated from below by a straight wire are studied. Two-dimensional flow ensues as density gradients are set up in the bulk liquid and surface tension gradients are set up in the interface. Surface profiles are measured experimentally using a reflecting schlieren technique. Profiles concave above the rising warm current are produced in the shallower pools and convex profiles in the deeper pools. The profile for intermediate depths is a hybrid with a shallow crest rising from a shallow trough. A mathematical model of the system is developed and yields numerical results in qualitative agreement with experiment. The importance of various fluid properties and system parameters on the surface profile is examined using further calculations based on the model.

1. Introduction

It is well known that, when natural convection occurs in a liquid pool heated from below or cooled from above, the free surface suffers slight deformations mirroring the flow beneath. Indeed it was the ingenious employment of such deformations that yielded many of Bénard's dramatic photographs of hexagonal cells in shallow layers of melted spermaceti heated from below. Bénard (1901) determined that the surface was concave above rising warm currents at the cell centres and convex along the cell boundaries where cooler liquid descended from the surface and that the elevation difference between cell centres and boundaries was of the order of one micron.

Theoretical examination of the surface relief problem has proceeded along two different lines, the first employing the approach of linear hydrodynamic stability analysis and the second seeking a simplified description of the developed steady-state flow.

Prediction of the free-surface configuration in the marginally stable state defined by linear stability analysis was first made by Jeffreys (1951) as a belated by-product of Rayleigh's original analysis of the stability of a fluid layer heated from below and subject to adverse density stratification. Jeffreys made the error of comparing his calculated results, based on the Rayleigh analysis, to Bénard's experiments, in which surface tension gradients rather than buoyancy forces

† Present address: Distillation Research Laboratory, Rochester Institute of Technology, Rochester, New York 14623.

were responsible for the convection. Not surprisingly, his calculations predicted surface deflexions opposite in sense to those reported by Bénard, i.e. convex over the warm rising currents and concave above descending ones, and he concluded that "Bénard's experimental work should be repeated". The analysis of instability driven by surface tension, apropos of Bénard's experiments, was made first by Pearson (1958), and the nature of the resulting surface deflexions was examined by Scriven & Sternling (1964), who found, as expected, that the surface should indeed be deflected in the sense observed by Bénard. Tacit in any such comparison of experiment to stability theory is the assumption that the same factors, particularly in this case the relative importance of surface tension and buoyancy forces, governing the onset of instability also pertain to the nature of the finite amplitude convection which ultimately develops. Making this assumption, Scriven & Sternling suggest that the sense of the surface deflexion in a given case might provide a useful experimental criterion for distinguishing convection driven by surface tension from that driven by buoyancy forces.

The results of stability analysis indicate further that, for a given liquid, the relative importance of surface tension and buoyancy forces depends on the pool depth, with the former predominating for most liquids when the depth is less than 1 mm and the latter controlling for depths greater than 1 cm. At intermediate depths both forces are important.

Experimental observations of surface relief have been reported for very shallow pools by Bénard (1901) and others (Block 1956; Volkovisky 1939). Surface relief in deep pools, on the other hand, has been reported by Spangenberg & Roland (1961) and Davidhazy (1969), all of whom observed deflexions in the sense predicted by Jeffreys. Apparently no reports showing *both* types of surface deflexion in a single study have been published, nor, in particular, has the transition that must exist between them as depth is increased from the regime of surface force dominance to that of buoyancy dominance been recorded.

The first objective of the present work is thus to construct a simple apparatus for the quantitative measurement of free-surface deformation during natural convection and to perform a set of experiments embracing both the surface tension and buoyancy dominated regimes. It is also desired to investigate, in terms of pool depth and fluid properties, the transition between the two different surface configurations characteristic of the two regimes.

2. Prediction of the magnitude of surface deformations

Since Bénard's early work, two highly simplified models have been proposed for predicting the difference in elevation between the centre and edge of Bénard's cells for fully developed steady flow. Hershey (1939), and later Anand & Karam (1969), assuming that the depth of the liquid pool increases linearly with distance from the centre of the cell and that a linear temperature gradient (i.e. a linear surface tension gradient) is imposed along the interface, apply solutions to the equations of motion for thermocapillary flow (cf. Levich 1962, p. 384). Hershey equates the lateral pressure difference resulting from the presence of thermocapillary flow to a change in hydrostatic head along the interface to give the

following expression for the difference in elevation from the centre to the edge of the cell:

$$\Delta h = 3\Delta\sigma/2\rho g h, \tag{1}$$

where h is the depth of pool, Δh the elevation difference between the cell centre and edge, $\Delta\sigma$ the difference in surface tension between centre and edge, ρ the liquid density and g the gravitational acceleration. For the conditions of Bénard's experiments, Hershey's model predicts elevation differences of approximately the magnitude observed experimentally but also predicts them to vary *inversely* with pool depth, contrary to the observations of Bénard. This results chiefly from failure to account for the effect of pool depth on heat transfer.

Anand, on the other hand, in seeking to determine elevation differences in molten Saran ® which was allowed to solidify, computes the total kinetic energy of the flowing system and equates it, upon solidification, to the change in potential energy resulting from the shift in centre of gravity associated with the deformation of the free surface. The resulting expression, when corrected for algebraic errors, is

$$\Delta h = \frac{h}{\mu}\frac{d\sigma}{dx}\left(\frac{0{\cdot}1h}{g}\right)^{\frac{1}{2}}, \tag{2}$$

where μ is the liquid viscosity. Although the correct order of magnitude is predicted for the elevation differences found in solidified Saran film, the equation must be questioned because its derivation treats the solidification as instantaneous and ignores the heat of fusion.

Both the above models treat the surface as wedge-shaped thereby assuming zero surface curvature and ignoring a possibly significant pressure term in the normal force balance. They are also inadequate for predicting the depth dependence of the elevation difference in pools heated from below since the associated thermal energy equation is not considered. Finally, they can be applied only for very shallow films since buoyancy forces are not considered in the flow equation.

The second objective of the present work is thus to develop a general theoretical model for predicting the surface configuration and the magnitude of the free-surface elevation difference accounting for heat transfer to and from the liquid pool, buoyancy forces and surface curvature. The model is restricted only in that it considers two-dimensional surface deformations. Such deformations are generated experimentally, however, so that comparison between experiment and theory can be made over a range of pool depths.

3. Apparatus and experimental procedure

An apparatus was constructed for generating and observing two-dimensional surface deformations accompanying the convective flow in liquid pools heated from below by means of a straight wire. The liquid pool test section is shown in figure 1. Liquid was added to a petri dish (15 cm in diameter, 2 cm deep) at the bottom of which was a quarter-inch thick polypropylene plate (12 cm in diameter). A thin groove was cut across the polypropylene plate and along this a 30-gauge nichrome wire was stretched. The wire was held taut between two leaf springs which took up thermal expansion in the wire during heating. The liquid pool

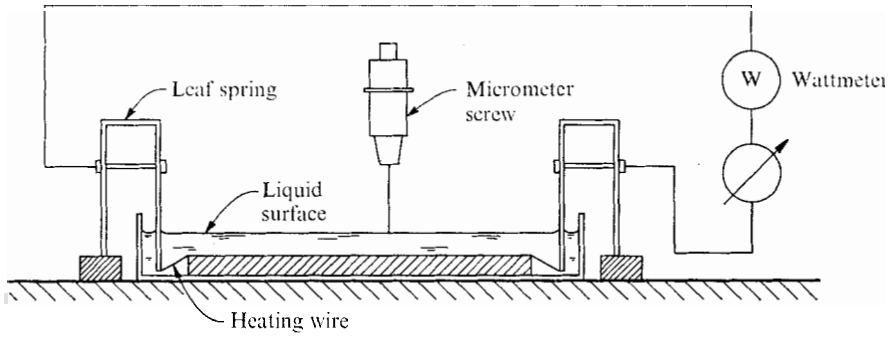

FIGURE 1. Schematic diagram of liquid pool test section.

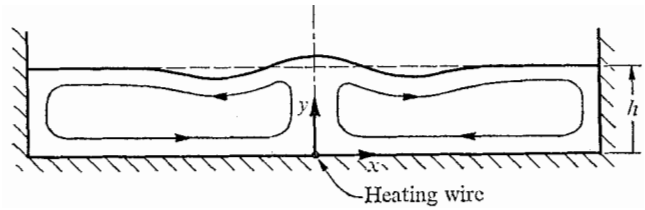

FIGURE 2. Schematic diagram of two-dimensional flow pattern established by the heating wire. Surface elevation differences greatly exaggerated.

depth was measured to within $\pm$ 0·005 cm with a micrometer screw as described elsewhere (Kayser 1971). Current was applied to the wire by a variac, and the power input was measured with a John Fluke Model 102 volt-ohm-watt meter. A two-dimensional cellular flow was produced in the liquid pool when power was supplied to the wire as shown in figure 2.

The experimental system employed is not directly analogous to that of Bénard's work in that hydrodynamic stability of the pool is not involved nor is the fluid required to descend near the wire as would be the case if a set of closely spaced parallel wires had been employed. Nevertheless, the systems are similar in that both produce steady currents of warm fluid ascending to the free surface from below.

Surface relief was determined for pools of a silicone fluid (200 centistoke Dow–Corning Series 200 fluid) and an aqueous glycerol solution (82 % glycerol by weight) at pool depths ranging from 0·185 to 0·658 cm. The fluid properties are summarized in table 1. It was necessary to use liquids of low volatility, to avoid evaporative convection, and high viscosity, to minimize the effects of room vibrations. The silicone oil was particularly advantageous since its low surface tension prevented its surface from becoming contaminated with traces of surfactant material. On the other hand, the glycerol solution had a high surface tension, and although the glycerol used was twice distilled and the water triply distilled, trace surface contamination was believed to be present, as demonstrated in hydrodynamic stability studies of the same solution (Palmer 1971). Depending upon pool depth, flow was induced by either or both the buoyancy and surface tension mechanisms. Above the wire, heated fluid rose to the surface, where

	Dow–Corning Series 200 silicone fluids (20 °C)†		82% by weight glycerol–water (25 °C)‡
Kinematic viscosity, ν (centistokes)	50	200	—
Viscosity, μ (cP)	48	194·2	75
Density, ρ (g/cm^3)	0·960	0·971	1·214
Thermal expansivity, α (°K^{-1})	0·00104	0·00096	0·000615
Thermal conductivity, k (cal/cm^2 s °K)	0·00036	0·00037	0·00076
Heat capacity, c_p (cal/gm °K)	0·37	0·355	0·604
Surface tension, σ (dyne/cm)	20·8	21·0	65·3§
$-d\sigma/dT$ (dyne/cm °K)	0·069	0·069	0·052§

† *Dow–Corning, Engineering Products Division Bull.* 05-136 (1965).

‡ *Physical Properties of Glycerine and Its Solutions*, Glycerine Producers Assoc., New York.

§ Measured in authors' laboratory.

TABLE 1. Physical properties of fluids used

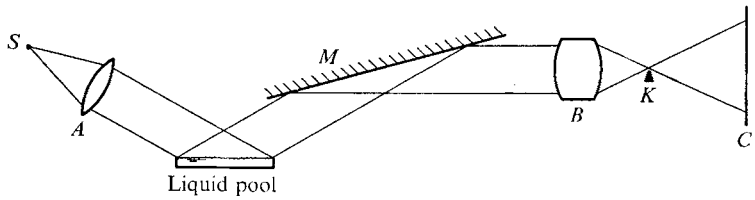

FIGURE 3. Schematic diagram of schlieren optical system showing light source S, condensing lens A, front surface mirror M, schlieren lens B, knife-edge diaphragm K and viewing screen C.

surface tension gradients, produced by the non-uniform heating and cooling of the surface, caused fluid to flow away from the centre of the liquid pool. The resulting surface deformations were two-dimensional, i.e. variations occurred normal to the liquid surface and perpendicular to the wire heater.

To observe and measure the deformation at the liquid surface, a reflecting schlieren system was employed, as shown in figure 3. Light from a rectangular tungsten ribbon source S was collimated by the condensing lens A, reflected from the liquid surface and focused by the schlieren lens B onto the focal plane K, where an image of the light source was formed. If the liquid surface was flat, the light rays reflected from it followed the standard optical axis, and the source image was formed at the point where this axis intersected the focal plane K. A light ray reflected from a sloping surface, as shown in figure 4, would be deflected from the optical axis by an angle $\Delta\epsilon$ equal to twice the angle the surface makes with the horizontal plane, i.e. twice the slope dh/dx. The source image formed by the deflected ray would then be displaced from the optical axis by a distance $\Delta z = F_2\Delta\epsilon = 2F_2(dh/dx)$, where F_2 is the focal length of the schlieren lens. The lens used had a focal length of 18 inches. A knife edge was positioned at K to block approximately half the source image formed by undeflected rays so that half the light passed onto the viewing screen C upon which the liquid

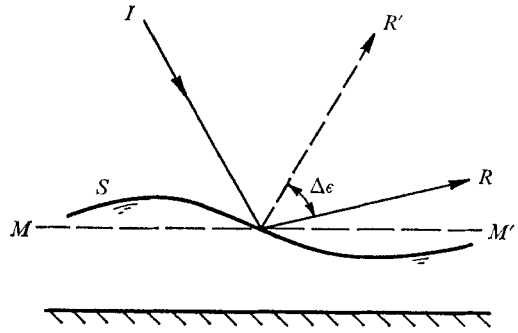

FIGURE 4. Reflexion of light ray from sloping liquid surface S. Incident ray I is reflected R at an angle of $\Delta\epsilon$ from the reflected ray R' that would have resulted if the surface were flat MM'.

surface was focused. Light rays reflected from an upward-sloping surface were thus blocked to an extent in direct proportion to the magnitude of the slope, and conversely for rays reflected from a downward-sloping surface. Typically, the viewing screen displayed a pattern of light and dark horizontal bands with the intensity of illumination at any point proportional to the surface slope at the corresponding position on the surface. The system was first calibrated, using a flat surface, by positioning the knife edge to block varying measured fractions of the source image and measuring the intensity of illumination at the viewing screen, i.e. photographic plate. Also, a reference photograph of the liquid surface was taken in each case before power was supplied to the wire heater. The surface was not strictly flat since the contact of the liquid with the walls of the container produced a shallow meniscus whose influence extended across the surface. Comparing the photograph of the deformed surface obtained when power was supplied to the heater with the reference photograph subtracted out meniscus effects as well as any effects of non-uniform surface illumination. Images of the surface were formed directly on the focal plane of a $2\frac{1}{4} \times 2\frac{1}{4}$ in. Hasselblad 1000F camera with the lens removed. Kodak Plus-X film was used and developed according to a standardized procedure, and unavoidable variations in film and processing were subtracted out by always using a reference negative. Optical density traces of both the reference and test negatives were made using a Joyce, Loebl & Co., Model MK111C automatic recording microdensitometer. Reliable correlation between optical density of the negatives and the intensity of the light received was of course restricted to the exposure range for which the two factors were proportional. Exposure times thus had to be carefully chosen. The apparatus and procedure, more details of which are given elsewhere (Kayser 1971), yielded reliable measurements of surface slopes between 0·5 and 45 μm/cm. The optical density traces were graphically integrated to yield the free-surface relief in each case.

Densitometer traces for a given negative, and hence measured surface slopes, were reproducible to within 3% of the full-scale variation of optical density, and these small uncertainties tended to cancel in the graphical integration. The greatest uncertainty lay in the necessarily arbitrary choice of the reference

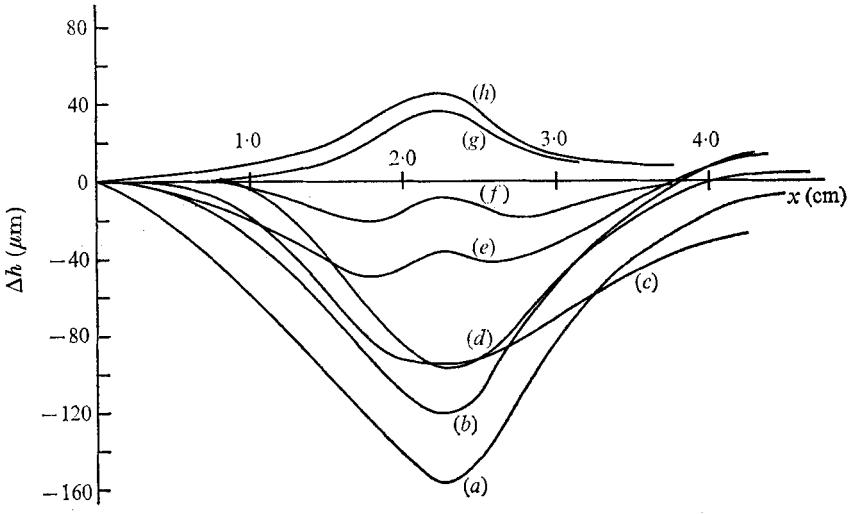

FIGURE 8. Surface profiles for pools of 200 centistoke Dow–Corning 200 fluid of varying depths heated from below by a wire. Pool depths (in cm) are (*a*) 0·218, (*b*) 0·257, (*c*) 0·304, (*d*) 0·346, (*e*) 0·407, (*f*) 0·44, (*g*) 0·505 and (*h*) 0·658.

optical density corresponding to a flat or undeflected surface. This reference point was taken in all cases to be at the edge of the surface corresponding to the left-hand sides of figure 5–10. Any difference in slope between the heated surface and the reference surface at this point would be propagated across the surface in the integration to obtain the surface profiles and thus led in many cases to the apparent failure of the surface elevation to return to the datum level, as shown in figures 8–10. While the uncertainty in choosing the reference point at which to initiate the integration of the densitometer traces may have led to errors of up to several microns in reported surface elevations, they would not alter the qualitative shape of the profiles.

4. Experimental results

Surface relief patterns were obtained for pools of the 200 centistoke Dow–Corning Series 200 silicone fluid at depths ranging from 0·218 to 0·658 cm. Power input to the heating wire was held constant at 0·50 watts. Representative schlieren photographs for depths of 0·257, 0·378 and 0·658 cm are shown in figures 5–7 (plates 1–3) together with diagrams showing the densitometer traces for the centre-line traverses and the corresponding surface relief for each case. The densitometer traverses obtained for the unheated reference surfaces are also shown for each case. Figure 8 shows surface profiles for all pool depths examined, and it is seen that in shallow pools ($h < 0{\cdot}35$ cm) the free surface is concave above the rising warm current whereas in deeper pools ($h > 0{\cdot}45$ cm) it is convex. The transition from the shallow-pool relief to the deep-pool relief is gradual rather than abrupt and presents a hybrid of the two patterns. The surface was deflected upward directly above the rising warm current, but this surface swelling resided at the centre of a broad surface trough.

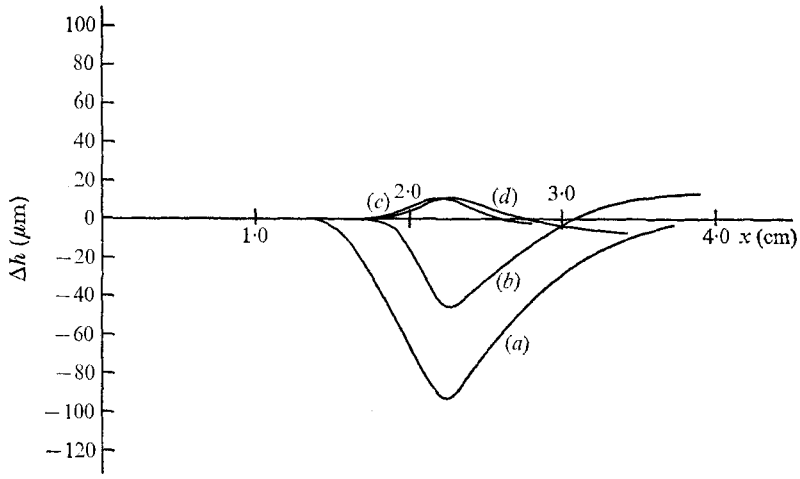

FIGURE 9. Surface profiles for pools of 82% by weight glycerol–water solutions of varying depths heated from below by a wire. Pool depths (in cm) are (*a*) 0·104, (*b*) 0·130, (*c*) 0·203 and (*d*) 0·259.

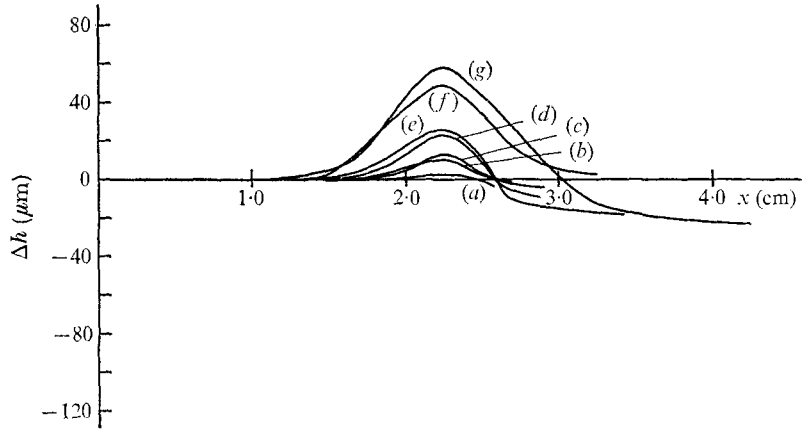

FIGURE 10. Surface profiles for pools of 82% by weight glycerol–water solutions of varying depths heated from below by a wire. A monolayer of oleic acid is spread on the surface. Pool depths (in cm) are (*a*) 0·130, (*b*) 0·155, (*c*) 0·188, (*d*) 0·216, (*e*) 0·236, (*f*) 0·267 and (*g*) 0·290.

The magnitude of the surface deflexions was of the order of 0–100 μm. In the shallower pools, the trough depth was inversely proportional to the pool depth in apparent disagreement with Bénard. This is not the case, however. The inverse dependence resulted from the intrusion of buoyancy effects even at the shallowest pool depths examined in this study. Attempts to form steady deflexions in extremely shallow pools such as those of Bénard ($h \leqslant 0{\cdot}1$ cm) led to the formation of dry patches over the wire. The convex deflexions generated in the deeper pools increased slightly over the range of depths examined. At intermediate depths, the surface became nearly flat.

Experiments with the aqueous glycerol solutions showed behaviour quali-

tatively similar to that of the silicone oil, but the transition from surface structure dominated by surface tension to buoyancy-dominated surface structure occurred at a much smaller pool depth and over a much narrower range of pool depths (0·13 cm $< h <$ 0·23 cm), as shown in figure 9. The difference in behaviour between the two liquids appears to be due not to differences in their fluid properties but rather to the partial contamination of the glycerol solution surface.

In a final set of experiments, the aqueous glycerol solution was intentionally covered with a surface active agent. 0·093 mg of oleic acid in a spreading solution of *n*-hexane was deposited on the surface, whose area was 225 cm^2, by means of a micrometer syringe. The oleic acid forms an expanded monomolecular film with a surface pressure of 22 dynes/cm on this solution at 23 °C (Lim 1971). The surfactant monolayer imparted the expected 'elasticity' to the surface and completely eliminated the surface tension mechanism for convection. At all pool depths, the only surface relief observed was convex above the rising current, as shown in figure 10.

5. Mathematical formulation

The model of the system studied, as shown in figure 2, consists of a pool of non-volatile liquid on top of a solid, horizontal, thermally insulated surface along which is located a line source of heat. The system is taken as infinite in the direction parallel to the line heat source but bounded by thermally insulated edges equidistant from the heat source on both sides of it. The ratio of the mean pool depth h to its width $2l$ is assumed to be small. Heat is lost from the free liquid surface in accordance with a general 'radiation' boundary condition. All fluid properties are taken as constant except surface tension and density, as it enters the gravitational term of the momentum equation. Both are taken to vary linearly with temperature.

The flow and temperature fields were first determined from the solution of the Navier–Stokes and thermal energy equations commensurate with the above model assuming the upper surface is flat. The surface pressure distribution derived from the above solution was then inserted into the normal force balance at the liquid surface, accounting for its slight deformation. The Navier–Stokes and thermal energy equations were put into the dimensionless forms

$$\left[\frac{\partial \Psi}{\partial x}\frac{\partial}{\partial y} - \frac{\partial \Psi}{\partial y}\frac{\partial}{\partial x}\right]\nabla^2\Psi = \nabla^4\Psi + Gr\frac{\partial \mathscr{T}}{\partial x},$$

$$Pr\left[\frac{\partial \Psi}{\partial x}\frac{\partial \mathscr{T}}{\partial y} - \frac{\partial \Psi}{\partial y}\frac{\partial \mathscr{T}}{\partial x}\right] = \nabla^2\mathscr{T} + Q_H, \tag{3}$$

respectively, where $Gr = \rho\alpha g T_0 h^3/\mu^2$, the Grashof number, reflects the extent of the contribution of buoyancy effects to the resulting convection and $Q_H = \phi h^2/kT_0$, the 'heating number', expresses the rate of energy supply from the line source. The equations were solved subject to the following boundary conditions:

$\Psi = 0$ (no flow across boundaries) on all boundaries,

$$\partial\Psi/\partial x = 0, \quad \partial\mathscr{T}/\partial x = 0 \text{ (symmetry) on } x = 0 \text{ for all } y,$$
$$\partial\Psi/\partial x = 0 \text{ (no slip)}, \quad \partial\mathscr{T}/\partial x = 0 \text{ (insulated edge) on } x = l/h \text{ for all } y,$$
$$\partial\Psi/\partial y = 0 \text{ (no slip) on } y = 0 \text{ for all } x,$$
$$\partial\mathscr{T}/\partial y = 0 \text{ (insulated boundary) on } y = 0 \text{ for all } x \neq 0,$$
$$\left.\begin{aligned} \partial^2\Psi/\partial y^2 &= Ma\,\partial\mathscr{T}/\partial x \quad \text{(tangential force balance)} \\ \partial\mathscr{T}/\partial y &= -Bi\mathscr{T} \quad \text{('radiation' condition)} \end{aligned}\right\} \text{ on } y = 1 \text{ for all } x.$$

These equations† were solved numerically using the CDC-6400 digital computer, yielding results for the flow field and temperature distribution. Details of the numerical methods used are given elsewhere (Kayser 1971). The solutions yielded the pressure distribution at the liquid surface to be substituted into the normal force balance, which in dimensionless form becomes

$$Su\frac{d^2\Delta\hbar}{dx^2} - Ga\,\Delta\hbar = -\not{p} + 2\frac{\partial^2\Psi}{\partial x\,\partial y}, \tag{4}$$

where the terms represent, from left to right, the normal force supporting surface curvature, the hydrostatic head, the normal pressure force and the normal viscous force.‡ Again, the individual variables are as defined in the first footnote below. The solution to (4), subject to boundary conditions

$$d\Delta\hbar/dx = 0 \quad \text{(symmetry)} \quad \text{on} \quad x = 0,$$
$$\Delta\hbar = 0 \quad \text{(reference)} \quad \text{on} \quad x = l/h,$$

was obtained, using variation of parameters, in the form

$$\Delta\hbar(x) = \frac{e^{bx} + e^{-bx}}{e^{bl/h} + e^{-bl/h}} \int_0^{l/h} \frac{f(\zeta)}{bs} \sinh b\left(\frac{l}{h} - \zeta\right) d\zeta + \int_0^{l} \frac{f(\zeta)}{bs} \sinh b(x-\zeta)\,d\zeta, \tag{5}$$

where $b = (Ga/Su)^{\frac{1}{2}}$ and $f(x) = -\not{p} + 2\,\partial^2\Psi/\partial x\,\partial y$.

Final results for the surface profile were obtained by performing numerically the integrations in (5).

6. Numerical results and discussion

Numerical calculations were made to examine the effect of several physical parameters on the surface configuration. In particular, calculations were made for a range of pool depths for systems whose properties coincided with those of the silicone fluid studied experimentally. Figure 11 shows half-profiles predicted

† x and y are the horizontal and vertical co-ordinates and $x = x/h$, $y = y/h$; u and v and $u = uh/\nu$ and $v = vh/\nu$ are the corresponding velocity components. T is temperature, T_0 initial temperature and $\mathscr{T} = (T - T_0)/T_0$. p is pressure, p_0 pressure at the undisturbed surface and $\not{p} = (p - p_0)h^2/p_0\nu^2$. ψ is the dimensionless stream function. $\hbar$ is the heat-transfer coefficient above the free surface, k thermal conductivity, α thermal expansivity, ν kinematic viscosity, κ thermal diffusivity, ρ_0 density at $T = T_0$ and ϕ the heat generation rate. $Pr = \nu/\kappa$, the Prandtl number; $Ma = -(\partial\sigma/\partial T)T_0 h/\mu\kappa$, the Marangoni number; $Bi = \hbar h/k$, the Biot number.

‡ In (4), $\Delta\hbar = \Delta h/h$, the non-dimensionalized surface deflexion; $Su = \sigma h/\rho\nu^2$, the Suratman number; $Ga = gh^3/\nu^2$, the Galileo number.

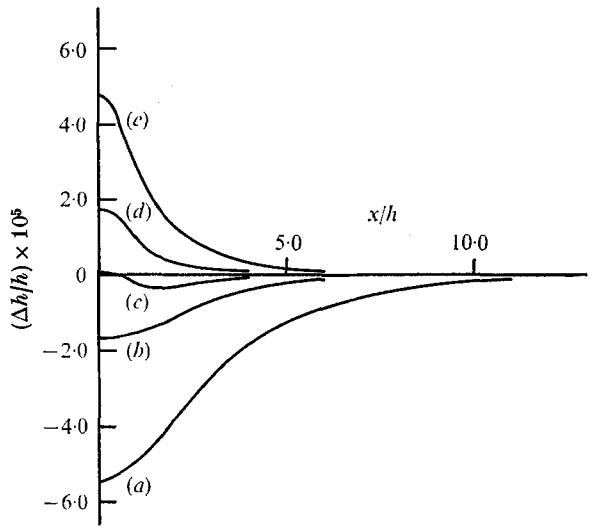

FIGURE 11. Calculated surface configurations for pools of 200 centistoke Dow–Corning Series 200 silicone fluid of various depths. $T_0 = 293$ °K, $\mathcal{h} = 0{\cdot}0003$ cal/cm² s °K, $\phi = 0{\cdot}243$ cal/cm³ s. Pool depths (in cm) are (*a*) 0·20, (*b*) 0·40, (*c*) 0·50, (*d*) 0·60 and (*e*) 0·80.

for 200 centistoke Dow–Corning Series 200 silicone fluid for depths ranging from 0·20 to 0·80 cm. The reference temperature was taken as 20 °C, and the heat-transfer coefficient in the air was taken as 0·0003 cal/cm² s °K, an estimate of the actual coefficient in the experiments. The heating rate used was 0·243 cal/cm³ s, corresponding to 0·00050 watts per cm of heating wire. This small value (in comparison with the experimental value of 0·033 W/cm) was used to avoid problems of stability and slow convergence in the numerical calculations. Nevertheless, comparison of the calculated results with the experimental results, shown in figure 8 in dimensionless co-ordinates, indicates that qualitative agreement was achieved despite the difference in heating rate and the somewhat arbitrary value chosen for the upper-surface heat-transfer coefficient. The experimentally observed transition in surface configuration with pool depth is replicated, and the magnitude of the calculated deflexions also agrees well with experiment. As shown in later calculations, changes in the heating rate had the effect of changing the amplitude of the surface deflexions without altering the shape of the profile. Thus, as expected, experimentally produced deflexions were approximately one hundred times larger than the calculated values.

Computations have shown that viscosity as well as surface tension has but a minor effect on the surface configuration. The physical properties of volumetric expansivity α and the temperature coefficient of surface tension $\partial\sigma/\partial T$ are the primary factors determining the relative importance of buoyancy and surface tension forces. Thus, as expected, these properties have a significant influence on the surface configuration. Figure 12 shows configurations for various combinations of these properties when ascribed to a fluid whose other properties are those of 50 centistoke Dow–Corning Series 200 fluid.

The rate of heat supply along the wire and the heat-transfer coefficient at the

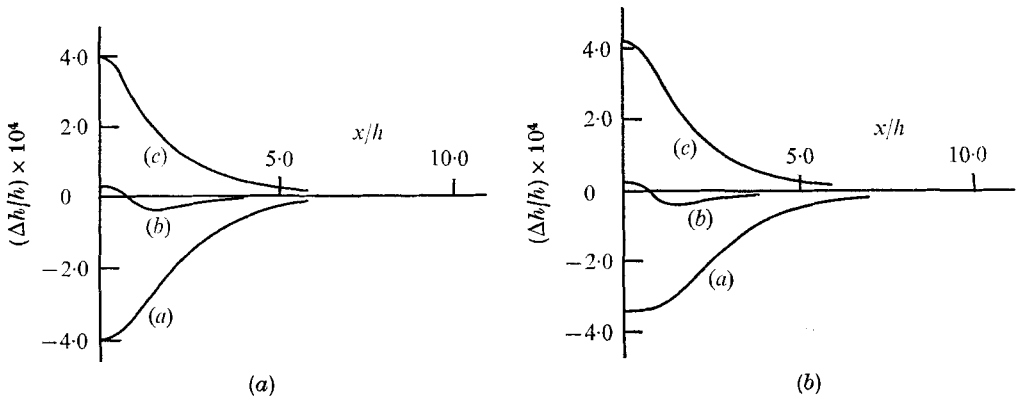

FIGURE 12. (*a*) Calculated surface profiles showing effect of α. Fluid properties are those of 50 centistoke Dow–Corning Series 200 silicone fluid except that the thermal expansivity for curves (*a*), (*b*) and (*c*) is put at 0·00000, 0·00104 and 0·00208 °K^{-1}, respectively. Pool depth is 0·50 cm, and heating conditions are the same as those for figure 11. (*b*) Calculated surface profiles showing effect of $d\sigma/dT$, which for curves (*a*), (*b*) and (*c*) is 0·138, 0·069 and 0·000 dynes/cm °K, respectively.

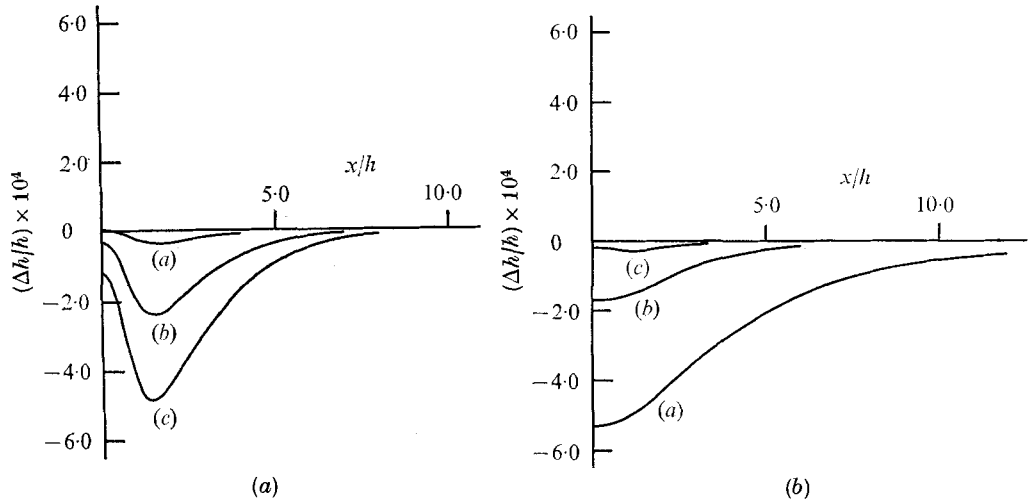

FIGURE 13. (*a*) Calculated surface profiles showing effect of heating rate. Fluid properties and conditions are the same as those for figure 11 except that the heating rate for curves (*a*), (*b*) and (*c*) is put at 2·434, 1·217 and 0·243 cal/cm^3 s. Pool depth is 0·50 cm. (*b*) Calculated surface profiles showing effect of heat-transfer coefficient above surface. h for curves (*a*), (*b*) and (*c*) is $6{\cdot}0 \times 10^{-5}$, $3{\cdot}0 \times 10^{-4}$ and $1{\cdot}5 \times 10^{-3}$ cal/cm^2 °K.

upper surface are also very important in determining the surface configuration. Figure 13(*a*) shows that, while changing the heating rate does not alter the importance of buoyancy relative to surface tension, it strongly influences the magnitude of the deflexions. On the other hand, the magnitude of the heat-transfer coefficient at the upper surface for a given liquid pool determines the importance of buoyancy relative to surface tension, as illustrated in figure 13(*b*). When the rate of heat loss from the upper surface is increased, the normal and

tangential temperature gradients are not proportionally increased. With an increased heat-transfer coefficient at the surface, the enhanced heat losses result in reduced temperature gradients along the surface and therefore reduced surface tension gradients. Temperature gradients normal to the surface, however, are increased by the greater heat losses at the surface producing increased density gradients in the bulk of the liquid. Since buoyancy forces increase and surface tension forces decrease with enhanced heat loss rate, the transition surface configuration is made to occur at a shallower pool depth. Thus under these conditions, the magnitude of the surface deflexions may be reduced by increasing the rate of surface cooling.

Calculations were not made for fluids with properties replicating the aqueous glycerol solutions, for which some experimental results were obtained. The chief difference between the aqueous glycerol and the silicone oil pools observed experimentally was the shallower transition depth, 1·8 mm, of the aqueous glycerol pool compared with 3·5 mm for the silicone fluid. The experimental conditions were identical in the two situations. One might expect to interpret the difference in terms of a difference in the importance of surface tension relative to buoyancy forces in the two cases as expressed by comparing the ratios of the Marangoni number to Grashof number in the two pools, i.e. Ma/Gr. If the temperature gradients in the two pools are the same, this ratio should be the same for a given surface configuration. Specifically, if $(Ma/Gr)_1 = (Ma/Gr)_2$, then the ratio of transition depths in the two pools is given by:

$$\frac{h_1}{h_2} = \left(\frac{(d\sigma/dT)_1 \rho_2 \alpha_2}{(d\sigma/dT)_2 \rho_1 \alpha_1}\right)^{\frac{1}{2}}.$$

This ratio is approximately unity for the two systems studied, so that the explanation for the discrepancy lies elsewhere. It is probably traceable to the fact that the glycerol solution, having a high surface tension, is easily contaminated. The effect of a trace contaminant on the surface, although not in a sufficiently high concentration to render the surface completely rigid, results in a reduction in the surface tension driving force produced by temperature gradients in the surface. Buoyancy forces therefore become relatively more important, resulting in a decrease in the transition depth, as observed.

A detailed analysis of the surface relief of pools supporting films of surface active materials would be an important extension of the present work.

For purposes of comparing results based on the present model with those predicted by Hershey and observed by Bénard, calculations were carried out for pools of varying depth in which buoyancy forces were absent. Hershey predicted for this case, with constant heat flux, that the magnitude of the surface depressions should decrease as pool depth increases, in contradiction to Bénard's observations. Computations for pools of a liquid whose properties are those of 50 centistoke Dow–Corning Series 200 fluid with the thermal expansivity α set equal to zero, however, show that the depth of the depression increases with pool depth, in agreement with Bénard.

7. Conclusions

Experiments employing a reflecting schlieren technique have yielded profiles of surface relief for shallow liquid pools heated from below by a single straight wire. The resulting two-dimensional natural convection produced a depression above the rising warm current in the shallower pools and a crest in the deeper pools, in agreement with the suggestions of earlier linear stability analyses of liquid pools heated from below. The transition with pool depth from a concave to a convex surface was gradual and characterized by a hybrid profile of a shallow crest rising from the centre of a shallow trough. Pools consisting of a 200 centistoke Dow–Corning silicone fluid as well as 82 % by weight glycerol–water solutions were used in the study; for the heating rates employed, the former showed transition at a depth of 0·35 cm and the latter at 0·18 cm. The trough-to-crest elevation differences were in the range of 0–100 μm. Experiments in which a monolayer of oleic acid was spread on the surface of the glycerol solution showed only the convex surface configuration.

A mathematical model of the heated pool was developed, and numerical results were obtained for the temperature and velocity distributions and for the free-surface profile under a variety of conditions. The predicted surface profiles showed qualitative agreement with experiment. Further calculations indicated that the thermal expansivity and the temperature coefficients of surface tension were the primary determiners of the shape of the surface profile, while viscosity and surface tension had only secondary effects. Increasing the heating rate exaggerated the surface elevation differences but did not change the shape of the surface, while increasing the efficiency of heat transfer away from the upper surface diminished lateral temperature differences, and hence surface tension differences, and shifted the surface profile to one characteristic of deeper pools, i.e. one in which buoyancy forces were more important than surface tension forces.

This work was supported in part by a grant from the National Science Foundation and a grant from the Office of Saline Water.

REFERENCES

ANAND, J. N. & KARAM, H. J. 1969 *J. Colloid Interface Sci.* **31**, 196.
BÉNARD, H. 1901 *Ann. Chim. Phys.* **23**, 62.
BLOCK, M. J. 1956 *Nature*, **178**, 529.
DAVIDHAZY, A. 1969 *Photographic Sci. Engng*, **13**, 156.
HERSHEY, A. V. 1939 *Phys. Rev.* **56**, 204.
JEFFREYS, H. 1951 *Quart. J. Mech.* **4**, 283.
KAYSER, W. V. 1971 Ph.D. dissertation, University of Washington.
LEVICH, V. G. 1962 *Physicochemical Hydrodynamics*. Prentice Hall.
LIM, Y. C. 1971 Ph.D. dissertation, University of Washington.
PALMER, H. J. 1971 Ph.D. dissertation, University of Washington.
PEARSON, J. R. A. 1958 *J. Fluid Mech.* **4**, 489.
SCRIVEN, L. E. & STERNLING, C. V. 1964 *J. Fluid Mech.* **19**, 321.
SPANGENBERG, W. B. & ROLAND, W. R. 1961 *Phys. Fluids*, **4**, 743.
VOLKOVISKY, V. 1939 *Publ. Sci. Tech. du Minist. de l'Air*, no. 151.

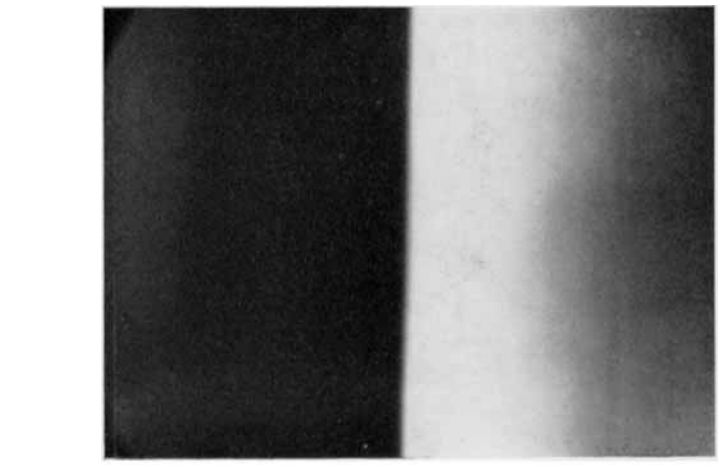

(*a*)

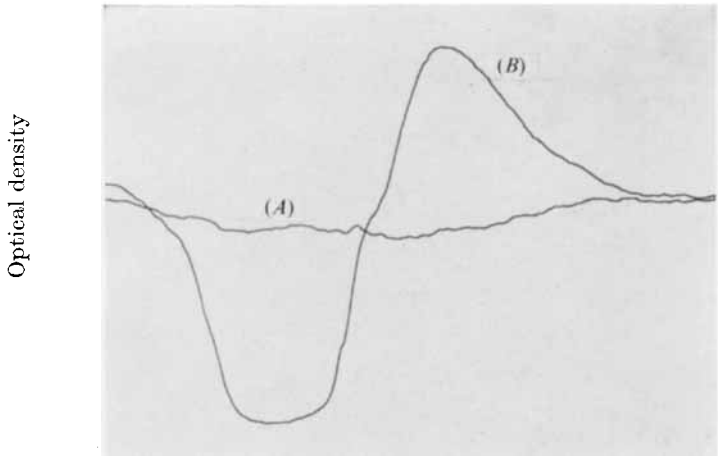

(*b*)

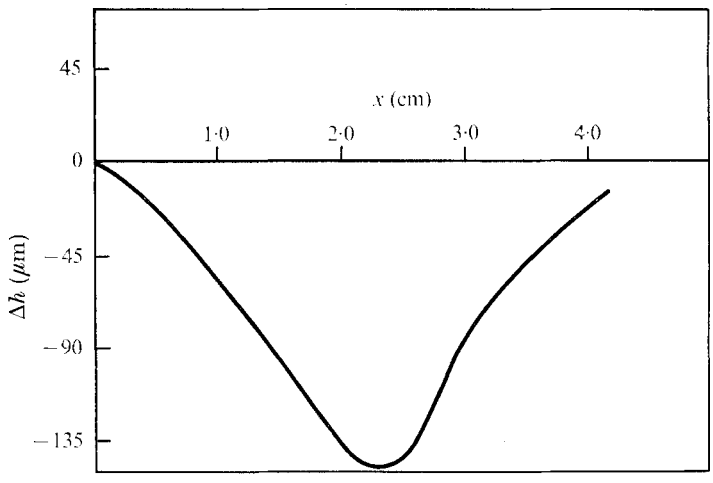

(*c*)

FIGURE 5. (*a*) Schlieren photograph, (*b*) optical density traverse and (*c*) surface elevation profile for 200 centistoke Dow–Corning 200 silicone fluid pool, depth 0·218 cm, heated from below by wire. The optical density traverse (*B*) of the unheated reference surface is shown together with the traverse (*A*) for the heated pool. Pool width shown is 5 cm.

(*a*)

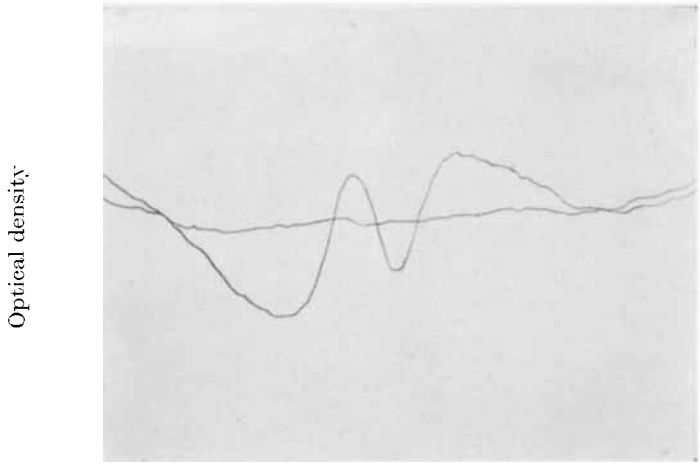

(*b*)

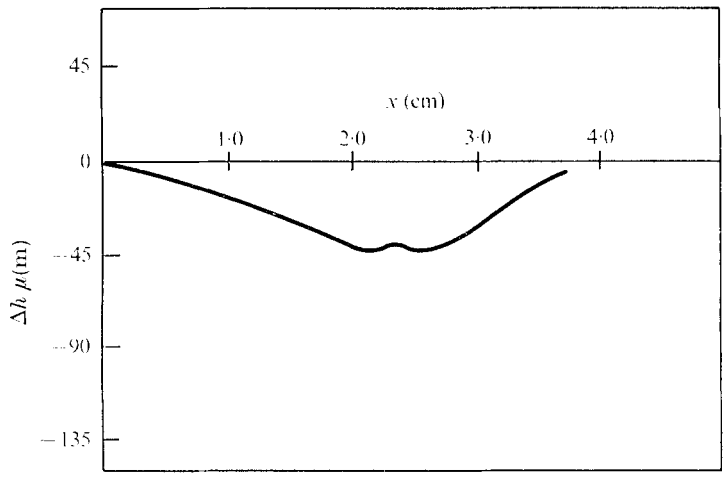

(*c*)

FIGURE 6. (*a*) Schlieren photograph, (*b*) optical density traverse and (*c*) surface elevation profile for 200 centistoke Dow–Corning 200 silicone fluid, pool depth 0·378 cm, heated from below by wire. Pool width 5 cm.

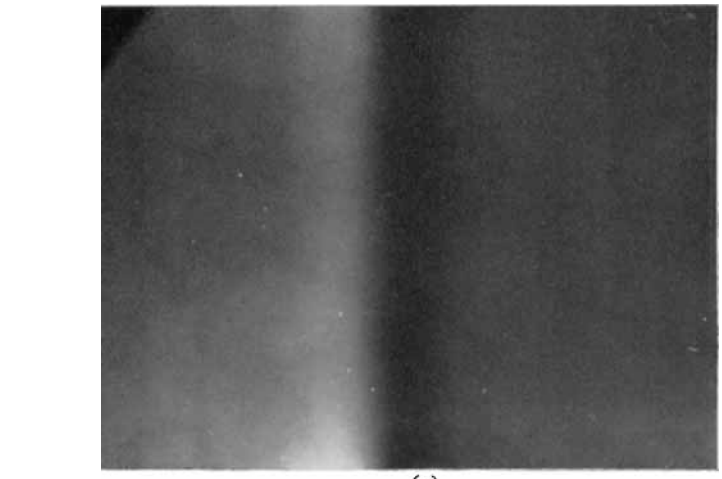

(*a*)

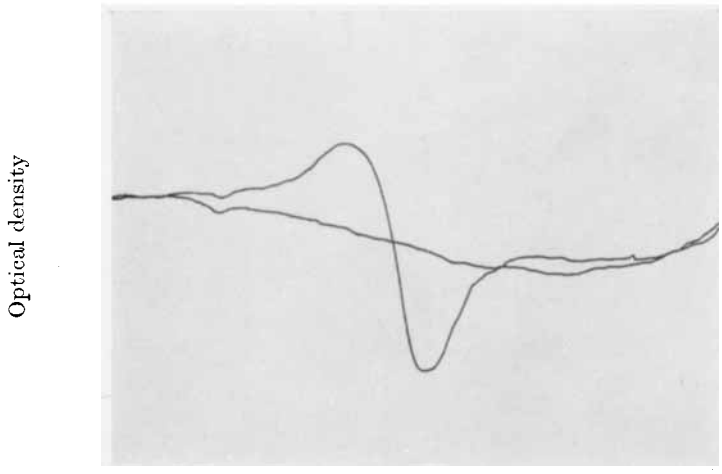

(*b*)

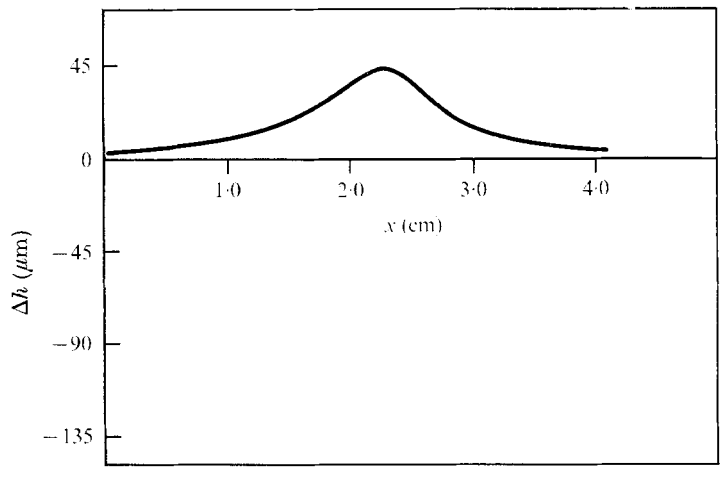

(*c*)

FIGURE 7. (*a*) Schlieren photograph, (*b*) optical density traverse and (*c*) surface elevation profile for 200 centistoke Dow–Corning 200 silicone fluid pool, depth 0·658 cm, heated from below by wire. Pool width 5 cm.